ACS EARTH AND SPACE CHEMISTRY

Open Access

http://pubs.acs.org/journal/aesccq

Article

Modeling an S_N2 Reaction Mechanism for Hydrolysis of Siloxane Linkages with Density Functional Theory under Basic Conditions and Implications for Dissolution of Quartz

Heath D. Watts and James D. Kubicki*

Cite This: *ACS Earth Space Chem.* 2026, 10, 1210–1215

Read Online

ACCESS | Metrics & More | Article Recommendations | Supporting Information

ABSTRACT: An extended silicate molecular cluster was used to perform density functional theory calculations to determine if an S_N2 mechanism, where OH^- attacks a Q^1 Si coupled with Na^+ charge balancing an adjacent siloxane bridging O atom, could explain the observed energy of activation of quartz dissolution under basic conditions.

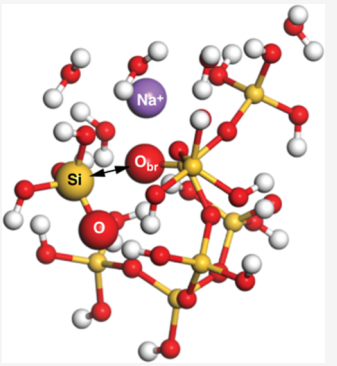

KEYWORDS: *hydrolysis, dissolution, weathering, density functional theory, silica, rates*

INTRODUCTION

The topic of silica and silicate dissolution rates concerns soil productivity,[1,2] corrosion of man-made materials,[3] biogeochemical cycles,[4,5] and geothermal energy extraction.[6−10] Numerous studies to determine the rates and mechanisms of silica and silicate dissolution, including laboratory, field, and *computational chemistry studies*, have been published. However, significant reaction rate discrepancies have resulted in laboratory,[11−16] field-laboratory,[17−20] simulation studies[21−39] and field-laboratory-simulation studies.[40−42]

There has been a lack of scientific agreement regarding the mechanism of quartz dissolution at the molecular level. However, our recent paper that used DFT calculations to obtain the activation energy (ΔE_a) of silica dissolution under acidic conditions using a novel reaction mechanism showed good agreement with reliable experimental data,[43] which provides a direction for this work. The current hypothesis suggests that the rate-limiting step is Si−O_{br}−Si linkage hydrolysis (O_{br} for "bridging O atom" hereafter). No other viable reaction has been shown that can lead to aqueous $Si(OH)_4$ through the transformation of 4 Si−O_{br}−Si linkages in silicate or silica. Here, we focused on modeling the Si−O_{br}-Si hydrolysis reaction while attempting to discover a reaction pathway that agrees with the observed silica dissolution (ΔE_a). If we can determine a reaction pathway that is consistent with experiment, it could be possible to predict hydrolysis rates and dissolution over a range solution compositions and temperatures, which could be applied to weathering, where rates are slow. The results from our work could also be applicable to subsurface reactions at higher T and higher ionic strength.

There is a large amount of experimental data related to silica dissolution and weathering, so we are citing a review that covers this topic.[42] Instead, we chose two papers that provide ΔE_a that we targeted with our work. Davis (2011) used a potentiometric technique and reported ΔE_a values of 29 and 37 kJ·mol^{-1} for dissolution at Q^1 and Q^2 Si sites, respectively.[15] Casey (1990) used isotopic dissolution rate measurements and found a ΔE_a of 36 kJ·mol^{-1} for quartz powder.[38]

Casey et al. (1990) first used quantum chemistry calculations to study the hydrolysis of Si−O−Si during silica dissolution. They found that their modeled H−D kinetic isotope effects differed drastically from experimental data, thus showing that proton transfer to the O_{br} was not the rate-limiting step in dissolution. Similar studies with small models continued for decades, and activation energies obtained from those studies were much higher than experimental data (e.g., Criscenti et al., 2006, where ΔE_a = 112 kJ·mol^{-1} under acidic conditions).[28] An early work used the ab initio calculations and reported a ΔE_a of 79 kJ·mol^{-1}.[44] A prior study with ab initio

Received: November 17, 2025
Revised: April 21, 2026
Accepted: April 22, 2026
Published: April 28, 2026

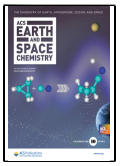

and DFT methods found energies of activation ranging from 71 to 73 kJ·mol^{-1}, depending on the method used on β-cristobalite surfaces.[45] Recently, others have used machine learning techniques to obtain ΔE_a from data to predict ΔE_a values of 79 and 84 kJ·mol^{-1} at pH 13 and 1 bar pressure, depending on the model used.[40] Kinetic Monte Carlo methods use experimental ΔE_a to attempt to predict phenomena consistent with observed dissolution rates, reporting activation energies from 93.1 ± 0.3 to 96.2 ± 0.03 kJ·mol^{-1}, dependent on the quartz surface used for the model.[36]

Our previous work showed that a Cl^- ion interacting with protonated O_{br} stabilized the model during dissolution.[43] Here, we focus on the interaction of aqueous Na^+ with O_{br} and a proposed hydrolysis reaction under basic conditions. Our calculations predicted that rather than direct attack of OH^- from solution to form a 5-coordinate surface Si ($^{[5]}$Si), OH^- could diffuse into the silica surface and form $^{[5]}$Si.[43] The OH^- attacks the Q^1 Si from below, resulting in a dissolved $Si(OH)_4$ leaving group through a similar S_N2 mechanism.

METHODS

All models were built using Materials Studio 2016 (Biovia, Inc.; San Diego, CA) and were energy-minimized using Gaussian 16.[46] The model stoichiometry was $Si_8O_{31}H_{29}Na$; our model is shown in Figure 1. In our previous paper,[43] where discussed silica dissolution under acidic conditions, we justified using this model because our model accurately reproduced quartz Si−O bond lengths and Si−O−Si bond angles, and by citing the results of Gibbs (2006) that used a model of similar size to our model.[47] Our model represents a general silicate that exhibits a Q^1 Si, where we hypothesize that dissolution can occur through OH^- attack on the Q^1 Si and cleavage of the Si−O_{br} bond. We extracted our initial cluster structure from an unpublished periodic DFT simulation model. We added 5 H_2O molecules for hydration, and added one Na^+ to stabilize the bridging O atom (O_{br}) during the dissolution of the Q^1 Si leaving group. Our goal was to explore a reaction mechanism using a silica model in which OH^- attacks a Q^1 Si from below and breaks away from its adjacent O_{br} to form $Si(OH)_4$. If our activation energy results agree with those from the select experiment, then our mechanism could be applied to larger silica models and periodic models.

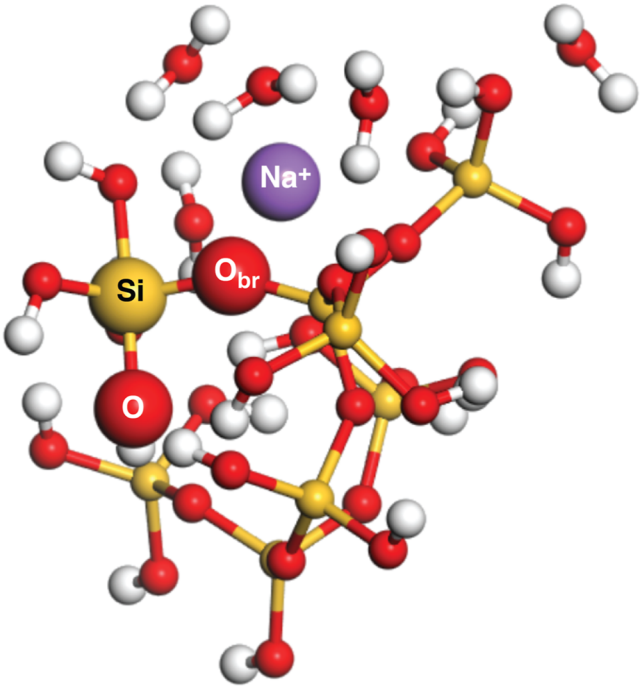

Figure 1. Model above shows a pentavalent Q^1 Si bonded to four OH^-, and an O_{br} between the Q^1 Si of interest and a Q^4 Si. A Na^+ is adjacent to the O_{br} to charge stabilize the O_{br}−$Si(OH)_4^-$ moiety during dissolution.

Energy minimization calculations were performed using density functional theory (DFT)[48,49] with the M06−2X functional.[50] We discussed our decision to choose the M06−2X functional in our paper about acidic silica dissolution based on that work and a paper cited therin.[43] The 6−311G(d,p) basis set was used for all calculations.[51] For the energy minimization calculations, we used an ultrafine integration grid and a fine CPHF grid.[46] After we geometry-optimized each model, we performed frequency calculation to affirm that each model was at a potential energy minimum and that each model exhibited real (>0 cm^{-1}) vibrational frequencies, or that the transition state model had one imaginary frequency (<0 cm^{-1}) associated with the Q^1 $Si(OH)_4$ and O_{br}.

We did not use implicit solvation for this work due to the results of test calculations in our prior related paper which showed that implicit solvation had an insignificant results on model energies.[43] Based on that work and prior experience, we think that it would be better to use larger models with increased explicit solvation or periodic models with explicit solvation to increase chemical accuracy rather than using implicit solvation.

For the stepwise dissolution calculations that were used to calculate the activation energy (ΔE_a), the minimized structure in Figure 1 underwent an incremental increase in the Q^1 Si−O_{br} distance until the $Si(OH)_4$ group dissociated from the cluster. For each stepwise dissolution calculation, the Si−O_{br} distance was maintained by freezing those two atoms and the distance between them by using the "-1" method in Gaussian 16,[46] whereas all of the other atoms were energy-minimized without constraining them. We energy-minimized the initial and final models of the stepwise calculations without constraining the distance between the O_{br} and the Q^1 Si. After finding the potential transition state model by constraining the Si−O_{br} distance, that model underwent a subsequent frequency calculation to determine whether the vibrational mode of interest (i.e., Si−O_{br}) gave one and only one imaginary frequency indicative of a saddle point on the potential energy surface.

For stepwise calculations, we set the energy of the fully minimized initial model to 0 kJ·mol^{-1} and reported the energies of the other models in the stepwise calculations relative to the initial model E. The E difference between the initial model and the transition state model gave the activation energy, ΔE_a.

Using ΔE_a, rate constants were calculated using eq 1:[52]

$$k_r = \frac{k_B T}{h}\frac{Q^{\ddagger}}{Q} e^{-\Delta E_a/k_B T} \quad (1)$$

In eq 1, k_r is the rate constant, k_B is the Boltzmann constant, h is Planck's constant, T is the temperature, and ΔE_a is the change in energy between the minimized reactant (initial) structure and the minimized transition state structure. $Q^{\ddagger}$ and Q are the v = 0 total partition functions of the transition state and reactant structures, respectively, which were obtained from Total V = 0 results from Gaussian 16 outputs for the initial and transition state models.[46]

Reaction rates were calculated using the rate law in eq 2:

$$\text{rate} = k_r(O_{br}\text{site density})(\%\ O_{br}) \quad (2)$$

In eq 2, k_r is the rate constant obtained from eq 1. O_{br} site density is estimated as 8 O_{br} sites per nm^2 from the quartz (101) model used to make our model in Figure 1,[22,37] and we calculate the % O_{br} with a plot of SiO^- surface site density percentage versus pH that was based on X-ray photoelectron spectroscopy (XPS) data from the literature.[53] The Carteisan coordinates and an image of the periodic quartz (101) structure are provided in the Supporting Information.

We used Materials Studio 2016 to determine the O_{br} and Na^+ distances from each of the stepwise, energy-minimized models.

https://doi.org/10.1021/acsearthspacechem.5c00356
ACS Earth Space Chem. 2026, 10, 1210−1215

RESULTS AND DISCUSSION

Figure 2 shows the relative electronic energy (E) compared with the lowest energy model configuration (Figure 2a), and

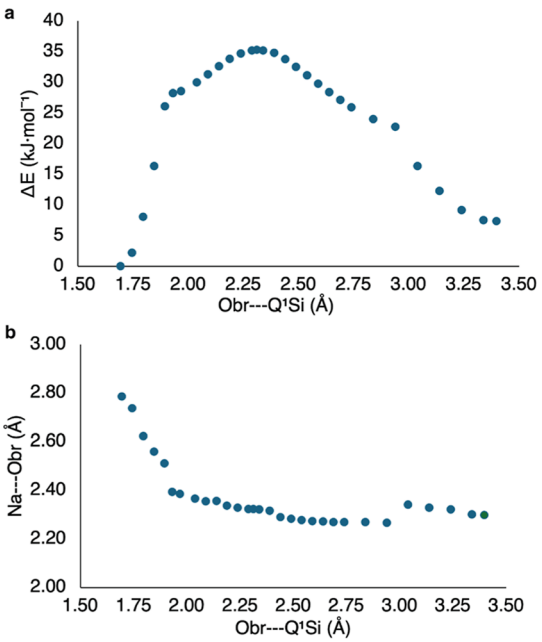

Figure 2. (a) Relative electronic energy (E) and (b) the O_{br}–Na^+ distance as the bond between the O_{br} and $Si(OH)_4$ increases and breaks.

the distance between O_{br} and Na^+ (Figure 2b) versus the distance between O_{br} and Q^1 Si. The Q^1 $Si(OH)_4$–O_{br} distance was constrained during each step of energy minimization dissolution calculations except for the first (1.69 Å) and last (3.40 Å) calculations that we minimized without constraints.

The plot in Figure 2a shows the trend in the energy change relative to the initial model as the $Si(OH)_4$–O_{br} bond distance increases incrementally, breaks, and dissociates. The overall reaction was mildly endothermic (i.e., ΔE of the reaction); the initial model had an energy that was 7 kJ·mol^{-1} lower than the energy of the final model. Our dissolution result under acidic conditions gave an exothermic reaction result, where ΔE of the reaction was −14 kJ·mol^{-1}.[43]

The model in Figure 3 has a 2.31 Å $Si(OH)_4$ –O_{br} distance and is the transition state model with one imaginary frequency for the $Si(OH)_4$–O_{br} vibrational mode at −131 cm^{-1}. The energy of that transition state model, compared to the first model, was 35 kJ·mol^{-1}, which agrees well with cited experimental data that we discussed in our introduction.[15] This result, coupled with the results from our work under acidic conditions,[43] shows that our proposed reaction mechanism could occur. DFT results have been found to have an uncertainty of approximately 10 kJ·mol^{-1};[54] however, even with that uncertainty level, our activation energy result is significantly lower than those previously reported from computational chemistry studies.

As the $Si(OH)_4$–O_{br} distance decreases, the distance between O_{br} and Na^+ decreases by about 0.5 Å (2.79 to 2.30 Å) (Figure 2c). This result suggests that Na^+ stabilizes the model by moving closer to O_{br} as that O becomes increasingly anionic during dissolution. To further evaluate this proposed

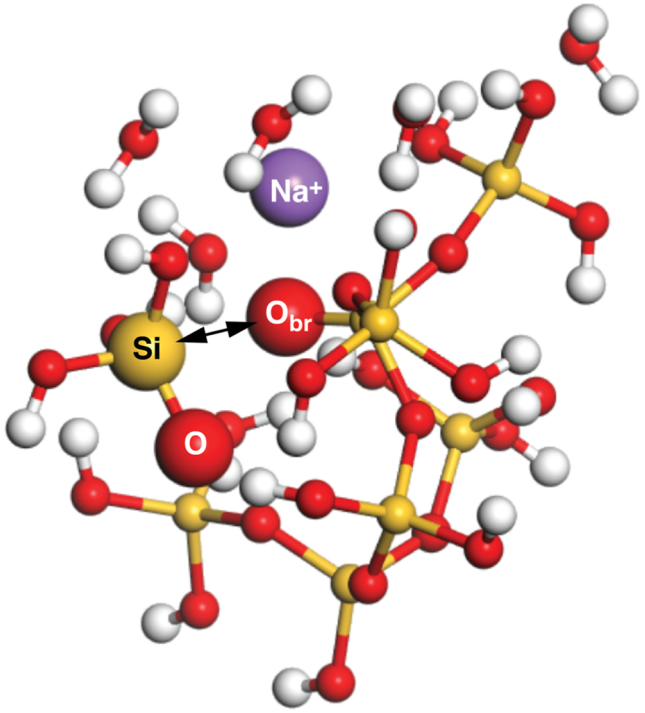

Figure 3. Transition state structure. The black, double-headed arrow shows the predominant vibrational mode at −131 cm^{-1} between O_{br} and the $Si(OH)_4$ leaving group.

phenomenon, we used two models (Figure 4): the first model (Figure 4a) where Na^+ is near O_{br} (2.79 Å) and the model in Figure 4b, where the distance between the Na^+ and O_{br} of interest was 3.90 Å. We found that the model where Na^+ was nearer to O_{br} of interest (Figure 4a) was 29 kJ·mol^{-1} lower in E than the model where Na^+ was far from O_{br}. This further shows that Na^+ interacting with the O_{br} of interest stabilized the model.

In Table 1, we show the calculated rate constants, k_r, that were obtained using eq 1 and compared with a select result.[55] We calculated our rate constants at 298.15 and 1.01 K and at 468.15 and 206 bar. We use the latter P and T to make our result pertinent to a 7450 m well UO_FU_5832_PT from the U.S. Department of Energy (US DOE) Forge (Frontier Observatory for Research in Geothermal Energy). Our k_r result at 298.15 K shows that our hypothesized reaction would proceed 5 × 10^3 times faster than the proposed reaction from previous model calculations.[55] The authors of the cited work used a smaller model that was charged ($Si_2O_8H_9^+$), whereas we used a larger, neutral model ($Si_8O_{31}H_{31}Cl$). These differences, coupled with the lack of the Na^+ counterion for charge balance and stability in the cited work,[55] could account for their different results. Note that our results are from harmonic frequency calculations; anharmonic frequency calculations can affect calculated reaction rates by one or more orders of magnitude.[56] This work and our previously published work show that our proposed mechanism provided results that agree better with experimental activation energies than prior computational chemistry studies, but future work with our proposed mechanism that calculates anharmonic frequencies might improve the accuracy of the results further.[43]

Using the rate constants from Table 1, a surface site density of 8 O_{br} per nm^2, and eq 2, the rates were calculated at 298.15

https://doi.org/10.1021/acsearthspacechem.5c00356
ACS Earth Space Chem. 2026, 10, 1210−1215

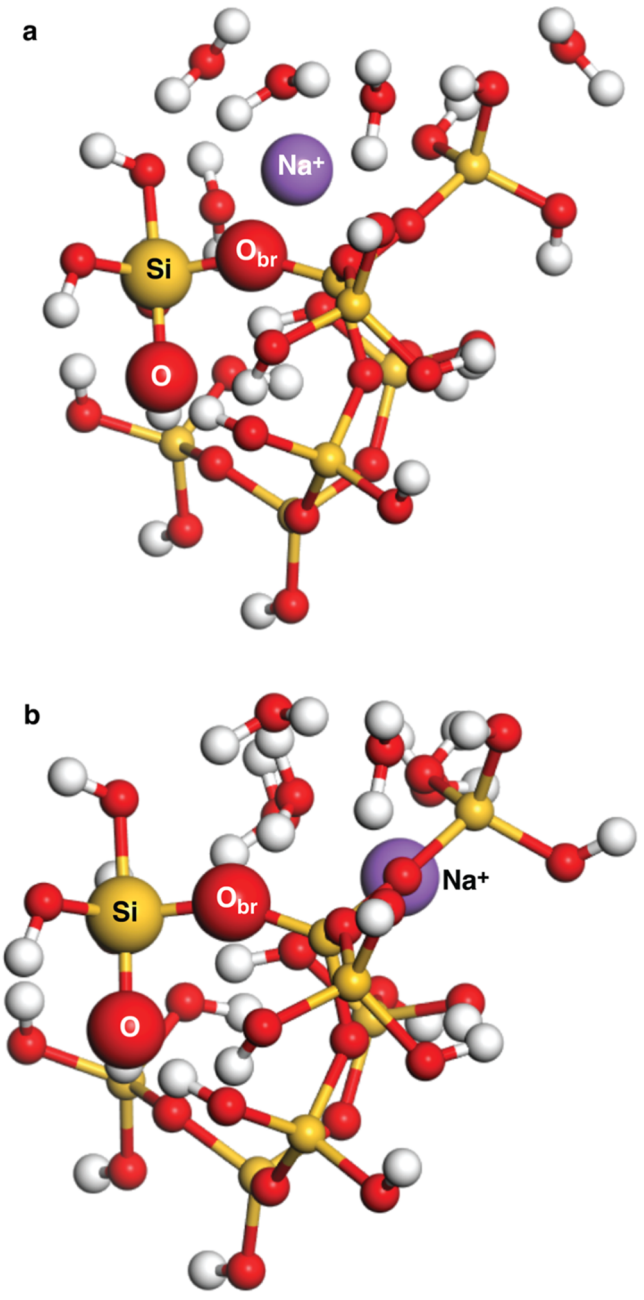

Figure 4. (a) Same as the model in Figure 1, whereas in (b), Na^+ was moved away from the O_{br} of interest. These models were used to evaluate the stabilizing effect of Na^+ on the models.

Table 1. Rate Constant, k_r, Results from This Work and Calculations Performed in Ref 55*[a]

temperature (K)	k_r (s^{-1})	Q	$Q^{\ddagger}$
298.15	5.20×10^{9}	1.87×10^{39}	2.42×10^{42}
468.15	2.97×10^{12}	1.59×10^{51}	4.22×10^{54}
298*	1.0×10^{6}*		

[a]The Q results for the reactant model (Q) and transition state model ($Q^{\ddagger}$) are from the Gaussian 16 log file results at the temperatures shown. Reference 55 did not report q results.

and 498.15 K (Table 2). As discussed in the Methods section, the % O_{br} site density was interpolated from XPS data.[53]

At both temperatures, Table 2 shows that as the increased (pH increase), the reaction rate increased. Furthermore, the rates at 468.15 K (i.e., geothermal conditions) are significantly faster than the rates at 298.15 K.

Table 2. Rate of the Dissolution Reaction as a Function of O_{br} Site Density Percentage (pH)

		T 298 K	T 468 K
pH	% O_{br}	rate (O_{br} sites·nm^{-2}·s^{-1}))	rate (O_{br} sites·nm^{-2}·s^{-1}))
8	20.0	8.31×10^{9}	4.74×10^{12}
9	22.9	9.50×10^{9}	5.42×10^{12}
10	25.7	1.07×10^{10}	6.10×10^{12}

Future work will include periodic structures that include surface defects where Q1 Si atoms are available to explore the dissolution mechanism proposed here more fully. The periodic structures will also allow a comparison of dissolution on different surfaces of the quartz model.

CONCLUSIONS

This work has shown that silicate dissolution under basic conditions could occur at Q^1 Si atoms by S_N2 attack if OH^- attacks from beneath the Si atom to form a $^{[5]}$Si. Concurrently, the O_{br} next to the Q^1 Si could be stabilized by Na^+ as dissolution occurs. We calculated an energy of activation of 32 kJ·moL^{-1}, which agrees more accurately with literature data than previous computational results. We calculated the rate constant and reaction rate results at 298.15 and 498.15 K, which could guide experiments and verify our hypothesized dissolution mechanism. These results for our proposed S_N2 mechanism show that as pH increases (at both 298.15 and 498.15 K), the dissolution rate increases.

ASSOCIATED CONTENT

Data Availability Statement

Data is provided within the manuscript.

Supporting Information

The Supporting Information is available free of charge at https://pubs.acs.org/doi/10.1021/acsearthspacechem.5c00356.

An image of the original periodic DFT simulation of a quartz (101)−water interface from which the molecular cluster used in this paper was derived, and a PDB format file of the structure (PDF)

AUTHOR INFORMATION

Corresponding Author

James D. Kubicki − *Department of Earth, Environmental and Resource Sciences, The University of Texas at El Paso, El Paso, Texas 79968, United States;* orcid.org/0000-0002-9277-9044; Email: jdkubicki@utep.edu

Author

Heath D. Watts − *Department of Earth, Environmental and Resource Sciences, The University of Texas at El Paso, El Paso, Texas 79968, United States;* orcid.org/0000-0001-6993-5398

Complete contact information is available at: https://pubs.acs.org/10.1021/acsearthspacechem.5c00356

Author Contributions

J.D.K. and H.D.W. designed the study. H.D.W. performed the calculations. H.D.W. and J.D.K. wrote and edited the manuscript.

Notes

The authors declare no competing financial interest.

■ ACKNOWLEDGMENTS

This work was funded by the U.S. Department of Energy, Office of Science, Energy Earthshots Initiatives under Award Number DE-SC0024703.

■ REFERENCES

(1) Swoboda, P.; Döring, T. F.; Hamer, M. Remineralizing Soils? The Agricultural Usage of Silicate Rock Powders: A Review; Elsevier B.V., 2022; p 150976. February 10..*Sci. Total Environ.*

(2) Schaller, J.; Puppe, D.; Kaczorek, D.; Ellerbrock, R.; Sommer, M. Silicon Cycling in Soils Revisited. *Plants*; MDPI AG, 2021; pp 1−36. February 1..

(3) Golovchak, R.; Kovalskiy, A.; Shpotyuk, Y.; Mahlovanyi, B.; Ploch, D.; Ignatova, T.; Kozdras, A.; Cebulski, J.; Czopek, S. Remedial Insight on Ageing of Glass through the Study of Ancient Man-made Artefacts. *Archaeometry* **2021**, *63* (2), 312−326.

(4) Tréguer, P. J.; Sutton, J. N.; Brzezinski, M.; Charette, M. A.; Devries, T.; Dutkiewicz, S.; Ehlert, C.; Hawkings, J.; Leynaert, A.; Liu, S. M.; Monferrer, N. L.; López-Acosta, M.; Maldonado, M.; Rahman, S.; Ran, L.; Rouxel, O. Reviews and Syntheses: The Biogeochemical Cycle of Silicon in the Modern Ocean. *Biogeosciences*; Copernicus GmbH, 2021; pp 1269−1289..

(5) Sutton, J. N.; André, L.; Cardinal, D.; Conley, D. J.; De Souza, G. F.; Dean, J.; Dodd, J.; Ehlert, C.; Ellwood, M. J.; Frings, P. J.; Grasse, P.; Hendry, K.; Leng, M. J.; Michalopoulos, P.; Panizzo, V. N.; Swann, G. E. A. A Review of the Stable Isotope Bio-Geochemistry of the Global Silicon Cycle and Its Associated Trace Elements; Frontiers Media S.A., 2018; . January 30..*Frontiers in Earth Science*

(6) Spitzmüller, L.; Goldberg, V.; Held, S.; Grimmer, J. C.; Winter, D.; Genovese, M.; Koschikowski, J.; Kohl, T. Selective Silica Removal in Geothermal Fluids: Implications for Applications for Geothermal Power Plant Operation and Mineral Extraction. *Geothermics* **2021**, *95*, 102141.

(7) Kamaratou, M.; Spinthaki, A.; Disci, D.; Demadis, K. D. Ferric Silicate Precipitates Relevant to Geothermal Systems: Delineation of Their Complex Formation. *Geothermics* **2024**, *123*, 103118.

(8) Spinthaki, A.; Petratos, G.; Matheis, J.; Hater, W.; Demadis, K. D. The Precipitation of "Magnesium Silicate" under Geothermal Stresses. Formation and Characterization. *Geothermics* **2018**, *74*, 172−180.

(9) Liu, S.; Ott, W. K. Sodium Silicate Applications in Oil, Gas & Geothermal Well Operations. *Journal of Petroleum Science and Engineering*; Elsevier B.V., 2020; p 107693..

(10) van den Heuvel, D. B.; Gunnlaugsson, E.; Gunnarsson, I.; Stawski, T. M.; Peacock, C. L.; Benning, L. G. Understanding Amorphous Silica Scaling under Well-Constrained Conditions inside Geothermal Pipelines. *Geothermics* **2018**, *76*, 231−241.

(11) Hamilton, J. P.; Pantano, C. G.; Brantley, S. L. Dissolution of Albite Glass and Crystal. *Geochim. Cosmochim. Acta* **2000**, *64* (15), 2603−2615.

(12) Dove, P. M.; Han, N.; Wallace, A. F.; De Yoreo, J. J. Kinetics of Amorphous Silica Dissolution and the Paradox of the Silica Polymorphs. *Proc. Natl. Acad. Sci. U. S. A.* **2008**, *105* (29), 9903−9908.

(13) Dove, P. M.; Han, N.; De Yoreo, J. J. Mechanisms of Classical Crystal Growth Theory Explain Quartz and Silicate Dissolution Behavior. *Proc. Natl. Acad. Sci. U. S. A.* **2005**, *102* (43), 15357−15362.

(14) Arvidson, R. S.; Luttge, A. Mineral Dissolution Kinetics as a Function of Distance from Equilibrium - New Experimental Results. *Chem. Geol.* **2010**, *269* (1−2), 79−88.

(15) Davis, M. C.; Wesolowski, D. J.; Rosenqvist, J.; Brantley, S. L.; Mueller, K. T. Solubility and Near-Equilibrium Dissolution Rates of Quartz in Dilute NaCl Solutions at 398−473K under Alkaline Conditions. *Geochim. Cosmochim. Acta* **2011**, *75* (2), 401−415.

(16) Icenhower, J. P.; Dove, P. M. The Dissolution Kinetics of Amorphous Silica into Sodium Chloride Solutions: Effects of Temperature and Ionic Strength. *Geochim. Cosmochim. Acta* **2000**, *64* (24), 4193−4203.

(17) Dove, P. M. Kinetic and Thermodynamic Controls on Silica in Weathering Environments. *Rev. Mineral.*; Mineralogical Society of America, 1995; Vol. *31*, pp 235−290..

(18) Rimstidt, J. D.; Barnes, H. L. The Kinetics of Silica-Water Reactions. *Geochim. Cosmochim. Acta* **1980**, *44* (11), 1683−1699.

(19) Zheng, X. Y.; Beard, B. L.; Johnson, C. M. Constraining Silicon Isotope Exchange Kinetics and Fractionation between Aqueous and Amorphous Si at Room Temperature. *Geochim. Cosmochim. Acta* **2019**, *253*, 267−289.

(20) Dove, P. M. The Dissolution Kinetics of Quartz in Aqueous Mixed Cation Solutions. *Geochim. Cosmochim. Acta* **1999**, *63* (22), 3715−3727.

(21) Adeagbo, W. A.; Doltsinis, N. L.; Klevakina, K.; Renner, J. Transport Processes at A-Quartz-Water Interfaces: Insights from First-Principles Molecular Dynamics Simulations. *ChemPhysChem* **2008**, *9* (7), 994−1002.

(22) Dellostritto, M. J.; Kubicki, J.; Sofo, J. O. Density Functional Theory Simulation of Hydrogen-Bonding Structure and Vibrational Densities of States at the Quartz (1 0 1)-Water Interface and Its Relation to Dissolution as a Function of Solution PH and Ionic Strength. *J. Phys.: Condens. Matter* **2014**, *26* (24), 244101.

(23) Nangia, S.; Garrison, B. J. Role of Intrasurface Hydrogen Bonding on Silica Dissolution. *J. Phys. Chem. C* **2010**, *114* (5), 2267−2272.

(24) Kubicki, J. D.; Sofo, J. O.; Skelton, A. A.; Bandura, A. V. A New Hypothesis for the Dissolution Mechanism of Silicates. *J. Phys. Chem. C* **2012**, *116* (33), 17479−17491.

(25) Pfeiffer-Laplaud, M.; Gaigeot, M. P. Adsorption of Singly Charged Ions at the Hydroxylated (0001) α-Quartz/Water Interface. *J. Phys. Chem. C* **2016**, *120* (9), 4866−4880.

(26) Pelmenschikov, A.; Leszczynski, J.; Pettersson, L. G. M. Mechanism of Dissolution of Neutral Silica Surfaces: Including Effect of Self-Healing. *J. Phys. Chem. A* **2001**, *105* (41), 9528−9532.

(27) Xiao, Y.; Lasaga, A. C. Ab Initio Quantum Mechanical Studies of the Kinetics and Mechanisms of Silicate Dissolution: H+(H3O+) Catalysis. *Geochim. Cosmochim. Acta* **1994**, *58* (24), 5379−5400.

(28) Criscenti, L. J.; Kubicki, J. D.; Brantley, S. L. Silicate Glass and Mineral Dissolution: Calculated Reaction Paths and Activation Energies for Hydrolysis of a Q 3 Si by H 3O + Using Ab Initio Methods. *J. Phys. Chem. A* **2006**, *110* (1), 198−206.

(29) Nangia, S.; Garrison, B. J. Reaction Rates and Dissolution Mechanisms of Quartz as a Function of PH. *J. Phys. Chem. A* **2008**, *112* (10), 2027−2033.

(30) Mahadevan, T. S.; Garofalini, S. H. Dissociative Chemisorption of Water onto Silica Surfaces and Formation of Hydronium Ions. *J. Phys. Chem. C* **2008**, *112* (5), 1507−1515.

(31) Nangia, S.; Garrison, B. J. Ab Initio Study of Dissolution and Precipitation Reactions from the Edge, Kink, and Terrace Sites of Quartz as a Function of PH. *Mol. Phys.* **2009**, *107* (8−12), 831−843.

(32) Lopes, P. E. M.; Demchuk, E.; Mackerell, A. D. Reconstruction of the (011) Surface on A-quartz: A Semiclassical *Ab Initio* Molecular Dynamics Study. *Int. J. Quantum Chem.* **2009**, *109* (1), 50−64.

(33) Lopes, P. E. M.; Murashov, V.; Tazi, M.; Demchuk, E.; MacKerell, A. D. Development of an Empirical Force Field for Silica. Application to the Quartz-Water Interface. *J. Phys. Chem. B* **2006**, *110* (6), 2782−2792.

(34) Leung, K.; Nielsen, I. M. B.; Criscenti, L. J. Elucidating the Bimodal Acid-Base Behavior of the Water-Silica Interface from First Principles. *J. Am. Chem. Soc.* **2009**, *131* (51), 18358−18365.

(35) Wallace, A. F.; Gibbs, G. V.; Dove, P. M. Influence of Ion-Associated Water on the Hydrolysis of Si-O Bonded Interactions. *J. Phys. Chem. A* **2010**, *114* (7), 2534−2542.
(36) Martin, P.; Gaitero, J. J.; Dolado, J. S.; Manzano, H. New Kinetic Monte Carlo Model to Study the Dissolution of Quartz. *ACS Earth Space Chem.* **2021**, *5* (3), 516−524.
(37) DelloStritto, M. J.; Kubicki, J. D.; Sofo, J. O. Effect of Ions on H-Bond Structure and Dynamics at the Quartz(101)-Water Interface. *Langmuir* **2016**, *32* (44), 11353−11365.
(38) Casey, W. H.; Lasaga, A. C.; Gibbs, G. V. Mechanisms of Silica Dissolution as Inferred from the Kinetic Isotope Effect. *Geochim. Cosmochim. Acta* **1990**, *54* (12), 3369−3378.
(39) Izadifar, M.; Ukrainczyk, N.; Koenders, E. Silicate Dissolution Mechanism from Metakaolinite Using Density Functional Theory. *Nanomaterials* **2023**, *13* (7), 1196.
(40) Gong, K.; Aytas, T.; Zhang, S. Y.; Olivetti, E. A. Data-Driven Prediction of Quartz Dissolution Rates at Near-Neutral and Alkaline Environments. *Front. Mater.* **2022**, *9*, 924834.
(41) Crundwell, F. K. On the Mechanism of the Dissolution of Quartz and Silica in Aqueous Solutions. *ACS Omega* **2017**, *2* (3), 1116−1127.
(42) Bañuelos, J. L.; Borguet, E.; Brown, G. E.; Cygan, R. T.; Deyoreo, J. J.; Dove, P. M.; Gaigeot, M. P.; Geiger, F. M.; Gibbs, J. M.; Grassian, V. H.; Ilgen, A. G.; Jun, Y. S.; Kabengi, N.; Katz, L.; Kubicki, J. D.; Lützenkirchen, J.; Putnis, C. V.; Remsing, R. C.; Rosso, K. M.; Rother, G.; Sulpizi, M.; Villalobos, M.; Zhang, H. Oxide- and Silicate-Water Interfaces and Their Roles in Technology and the Environment. *Chemical Reviews*; American Chemical Society, 2023; pp 6413−6544..
(43) Watts, H. D.; Kubicki, J. D. An SN2 Reaction Mechanism for Hydrolysis of Siloxane Linkages and the Implications for Dissolution of Quartz. *Sci. Rep.* **2025**, *15* (1), 42484.
(44) Xiao, Y.; Lasaga, A. C. Ab Initio Quantum Mechanical Studies of the Kinetics and Mechanisms of Quartz Dissolution: OH-Catalysis. *Geochim. Cosmochim. Acta* **1996**, *60* (13), 2283−2295.
(45) Pelmenschikov, A.; Strandh, H.; Pettersson, L. G. M.; Leszczynski, J. Lattice Resistance to Hydrolysis of Si - O - Si Bonds of Silicate Minerals: Ab Initio Calculations of a Single Water Attack onto the (001) and (111) β-Cristobalite Surfaces. *J. Phys. Chem. B* **2000**, *104* (24), 5779−5783.
(46) Frisch, M. J.; Trucks, G. W.; Schlegel, H. B.; Scuseria, G. E.; Robb, M. A.; Cheeseman, J. R.; Scalmani, G.; Barone, V.; Petersson, G. A.; Nakatsuji, H.; Li, X.; Caricato, M.; Marenich, A. V.; Bloino, J.; Janesko, B. G.; Gomperts, R.; Mennucci, B.; Hratchian, H. P.; Ortiz, J. V.; Izmaylov, A. F.; Sonnenberg, J. L.; Williams-Young, D.; Ding, F.; Lipparini, F.; Egidi, F.; Goings, J.; Peng, B.; Petrone, A.; Henderson, T.; Ranasinghe, D.; Zakrzewski, V. G.; Gao, J.; Rega, N.; Zheng, G.; Liang, W.; Hada, M.; Ehara, M.; Toyota, K.; Fukuda, R.; Hasegawa, J.; Ishida, M.; Nakajima, T.; Honda, Y.; Kitao, O.; Nakai, H.; Vreven, T.; Throssell, K.; Montgomery, J. A., Jr.; Peralta, J. E.; Ogliaro, F.; Bearpark, M. J.; Heyd, J. J.; Br; Kudin, K. N.; Staroverov, V. N.; Keith, T. A.; Kobayashi, R.; Normand, J.; Raghavachari, K.; Rendell, A. P.; Burant, J. C.; Iyengar, S. S.; Tomasi, J.; Cossi, M.; Millam, J. M.; Klene, M.; Adamo, C.; Cammi, R.; Ochterski, J. W.; Martin, R. L.; Morokuma, K.; Farkas, O.; Foresman, J. B.; Fox, D. J., et al. *Gaussian 16*; Gaussian, Inc.: Wallingford, 2016.
(47) Gibbs, G. V.; Jayatilaka, D.; Spackman, M. A.; Cox, D. F.; Rosso, K. M. Si-O Bonded Interactions in Silicate Crystals and Molecules: A Comparison. *J. Phys. Chem. A* **2006**, *110* (46), 12678−12683.
(48) Kohn, W.; Sham, L. J. Self-Consistent Equations Including Exchange and Correlation Effects. *Phys. Rev.* **1965**, *140* (4A), A1133−A1138.
(49) Hohenberg, P.; Kohn, W. Inhomogeneous Electron Gas. *Phys. Rev.* **1964**, *136* (3B), B864−B871.
(50) Zhao, Y.; Truhlar, D. G. The M06 Suite of Density Functionals for Main Group Thermochemistry, Thermochemical Kinetics, Noncovalent Interactions, Excited States, and Transition Elements: Two New Functionals and Systematic Testing of Four M06-Class Functionals and 12 Other Function. *Theor. Chem. Acc.* **2008**, *120* (1−3), 215−241.
(51) Krishnan, R.; Brinkley, J. S.; Seeger, R.; Pople, J. A. Self-consistent Molecular Orbital Methods. XX. A Basis Set for Correlated Wave Functions. *J. Chem. Phys.* **1980**, *72* (1), 650−654.
(52) Felipe, M.; Xiao, Y.; Kubicki, J. D. Molecular Orbital Modeling and Transition State Theory in the Geosciences. *Molecular Modeling Theory: Applications in the Geosciences, Reviews in Mineralogy and Geochemistry 42* **2001**, *42*, 485−531.
(53) Duval, Y.; Mielczarski, J. A.; Pokrovsky, O. S.; Mielczarski, E.; Ehrhardt, J. J. Evidence of the Existence of Three Types of Species at the Quartz-Aqueous Solution Interface at PH 0−10: XPS Surface Group Quantification and Surface Complexation Modeling. *J. Phys. Chem. B* **2002**, *106* (11), 2937−2945.
(54) Benisek, A.; Dachs, E. The Accuracy of Standard Enthalpies and Entropies for Phases of Petrological Interest Derived from Density-Functional Calculations. *Contrib. Mineral. Petrol.* **2018**, *173* (11), 90.
(55) Nangia, S.; Garrison, B. J. Reaction Rates and Dissolution Mechanisms of Quartz as a Function of PH. *J. Phys. Chem. A* **2008**, *112* (10), 2027−2033.
(56) Schmalz, F.; Kopp, W. A.; Kröger, L. C.; Leonhard, K. Correcting Rate Constants from Anharmonic Molecular Dynamics for Quantum Effects. *ACS Omega* **2020**, *5* (5), 2242−2253.

https://doi.org/10.1021/acsearthspacechem.5c00356
ACS Earth Space Chem. 2026, 10, 1210−1215